Applications and Applied Mathematics: An International Journal (AAM)

Volume 12 | Issue 1 Article 27

6-2017

Stability of Triangular Libration Points in the Sun - Jupiter System under Szebehely's Criterion

M. R. Hassan
S. M. College, T. M. Bhagalpur University

Md. A. Hassan
GTE, Yeshwanthpur

M. Z. Ali
Millia Convent School

Available at
http://pvamu.edu/aam
Appl. Appl. Math.
ISSN: 1932-9466

Applications and Applied Mathematics:
An International Journal
(AAM)

Vol. 12, Issue 1 (June 2017), pp. 415 - 432

Stability of Triangular Libration Points in the Sun - Jupiter System under Szebehely's Criterion

M. R. Hassan[1], Md. Aminul Hassan[2] and M. Z. Ali[3]

[1]P. G. Department of Mathematics
S. M. College, T. M. Bhagalpur University
Bhagalpur-812001, India
hassansmc@gmail.com

[2]GTE, Yeshwanthpur
Bangalore-560022, India
mahassan012@gmail.com

[3]Millia Convent School
Bhagalpur-812002, India

Received July 22, 2016; Accepted February 1, 2017

Abstract

In the present study, the classical fourth-order Runge-Kutta method with seventh-order automatic step-size control has been carried out to examine the stability of triangular libration points in the Sun-Jupiter system. The Sun is a highly luminous body and Jupiter is a highly spinning body, so radiation pressure of the Sun and oblateness of the Jupiter cannot be neglected. These factors must have some effects on the motion of the infinitesimal mass (spacecraft) and consequent effects on the stability of the triangular libration points. It is to be noted that in our problem, infinitesimal mass exerts no influence of attraction on the primaries (Sun and Jupiter) but its motion is influenced by the primaries. Therefore, the equations of motion of the infinitesimal mass moving in the gravitational field of the radiating Sun and oblate Jupiter have been established for numerical integration. To check the stability of the libration points, the infinitesimal mass is allowed to librate for trajectory generation in the vicinity of one of the triangular libration points. Using double-precision computation, the Jacobian constant was calculated in order to observe the validity of the trajectory generation throughout the numerical integration. This constant of integration was checked to make sure that it remained constant at least to eight decimal places, so that other data may be accurate. Following all the above computational techniques, the maximum displacement and maximum velocity envelopes were constructed in the light of previous authors. The reason behind the assumption of the maximum displacement and maximum velocity envelopes is that the spacecraft (infinitesimal mass) will librate for a long time within the region of the envelopes without crossing the *x*-axis. If the area of the envelope is not maximum within the given time limit and the infinitesimal mass crosses the *x*-axis, then by changing the initial conditions; we attempt to construct the envelopes of maximum area following previous authors. If the area of the envelope is maximum it means spacecraft

(infinitesimal mass) will librate in wider area for a long time without crossing the *x*-axis and longtime libration will give the higher range of stability. From our observation, it is found that due to the oblateness of Jupiter, the range of stability is reduced but photogravitation of the Sun has no significant effect on the triangular libration points.

Keywords: Restricted Three-body problem; Libration Points; Photogravitation; Oblateness; Critical mass; Poincare Surface of Section; Stability; Commensurability

MSC 2010 No.: 37M05, 70F07, 70F15

1. Introduction

Recently some space researchers are engaged in search of stable libration points to set a space station and parking zone for the space voyage and hence they are checking the stability of triangular libration points. In the Classical Restricted Three-body Problem, all collinear libration points are unstable but according to some authors, the triangular libration points are linearly stable whereas some authors established stability criteria as $\mu < \mu_c$, where μ_c is the critical mass of the restricted three-body problem. A series of works has been performed by Deprit et al. (1967). Markeev (1969), Alfriend (1970). Henrard (1970) established that in the vicinity of L_4, family of periodic orbits does not evolve in a continuous manner with the mass ratio. Nayfeh (1971) studied the problem with the help of commensurability 2:1 and 3:1. Markeev (1973) and Sokolski (1975) also studied the stability of the Langrage solution.

McKenzie and Szebehely (1981) defined a new criterion for the stability of the third body in the neighbourhood of the triangular libration points. For this, they defined maximum velocity and maximum displacement envelopes within which the third body remains for a long time starting from the suitable initial conditions, so that the third body may not cross the $x-$axis. This condition of not crossing the $x-$axis was introduced as the stability criteria for the third body. Tuckness (1995) investigated the sensitiveness of the third body numerically in the neighbourhood of L_4 by giving positional and velocity deviations from L_4 under some suitable initial conditions. He used Poincare's surface of sections to compare the periodic, quasi-periodic and chaotic regions of the trajectories with the definitions of stability given by McKenzie and Szebehely (1981).

Moreover, he also investigated the value of μ (the mass ratio) ranging from zero to critical mass $\mu_c = 0.038521....$. Using the stability criteria, he determined some values of μ for which libration points are more stable in comparison with the other values of μ. Markellos et al. (1996) and Papadakis (1998) studied the different aspects of non-linear stability of Lagrangian points in the plane Circular Restricted Three-body Problem. Zsolt Sandar et al. (2000) discussed phase-space structure in the vicinity of triangular libration points in the Restricted Three-body Problem. Hassan et al. (2013) extended the work of Tuckness (1995) by considering the effect of oblateness of the bigger primary and showed that with the increase of oblateness and commensurability, the critical mass reduces and the range of stability decreases accordingly. Tuckness (2005) established the valid stability criteria in the light of Syzygies especially in the Newtonian time domain. It projects new information about the stable motion of the third body.

In the present work, we propose to extend the work of Hassan et al. (2013) in the Sun-Jupiter system in the Restricted Three-body problem. Stability criteria given by McKenzie and Szebehely (1981) and computational techniques of Tuckness (1995) and Hassan et al. (2013) have been considered for discussing the problem.

2. Equations of Motion of the Infinitesimal Mass (Third Body)

In dimensionless variables, the equations of motion of the third body, in synodic co-ordinate system, in the gravitational field of the Sun and Jupiter are

$$\left.\begin{aligned} \ddot{x} - 2n\dot{y} &= \frac{\partial \Omega}{\partial x}, \\ \ddot{y} + 2n\dot{x} &= \frac{\partial \Omega}{\partial y}, \end{aligned}\right\} \tag{1}$$

where

$$\Omega = \frac{n^2}{2}\left[(1-\mu)r_1^2 + \mu r_2^2\right] + \frac{(1-p)(1-\mu)}{r_1} + \frac{\mu}{r_2} + \frac{3I}{2r_2^3}. \tag{2}$$

The mean motion "n" of the synodic frame is given by

$$n^2 = 1 + \frac{3I}{2}, \tag{3}$$

$I = A_e - A_p =$ Oblateness parameter of the smaller primary,

$A_e = \frac{b^2}{5R^2} =$ moment of inertia of the oblate body about the equatorial radius b,

$A_p = \frac{c^2}{5R^2} =$ moment of inertia of the oblate body about the polar radius c,

$R =$ the dimensional distance between the primaries,

$p =$ Radiation pressure of the Sun on the third body,

$r_1 = \left[(x-\mu)^2 + y^2\right]^{\frac{1}{2}} =$ the distance of the infinitesimal mass from the first primary and

$r_2 = \left[(x-\mu+1)^2 + y^2\right]^{\frac{1}{2}} =$ the distance of the infinitesimal mass from the second primary.

The equations in the System (1) can be reduced to a single equation

$$\dot{x}^2 + \dot{y}^2 = 2\Omega(x, y) - C,$$

i.e.,

$$F(x.y, \dot{x}, \dot{y}) = \dot{x}^2 + \dot{y}^2 - 2\Omega(x, y) + C = 0, \tag{4}$$

where C is called Jacobi constant and $F\left(x, y, \dot{x}, \dot{y}\right)$ is called Jacobi's manifold.

3. Triangular Libration Points

Since the triangular libration points are the singularities of the manifold $F\left(x, y, \dot{x}, \dot{y}\right) = 0$, hence the libration points are the solutions of the equations

$$\frac{\partial \Omega}{\partial x} = 0 \text{ and } \frac{\partial \Omega}{\partial y} = 0,$$

i.e.,

$$\frac{\partial \Omega}{\partial x} = n^2 x - \frac{(1-\mu)(x-\mu)(1-p)}{r_1^3} - \frac{\mu(x-\mu+1)}{r_2^3} - \frac{9I(x-\mu+1)}{2r_2^5} = 0 \tag{5}$$

and

$$\frac{\partial \Omega}{\partial y} = y\left[n^2 - \frac{(1-\mu)(1-p)}{r_1^3} - \frac{\mu}{r_2^3} - \frac{9I}{2r_2^5}\right] = 0. \tag{6}$$

Equation (5) $-$ Equation (6)$\times(x-\mu+1)$ gives

$$n^2 = \frac{1-p}{r_1^3}. \tag{7}$$

Equation (5) $-$ Equation (6)$\times(x-\mu)$ gives

$$n^2\mu - \frac{\mu}{r_2^3} - \frac{9I}{2r_2^5} = 0. \tag{8}$$

Finally, the triangular libration points are the solutions of the equations

$$-n^2 + \frac{1-p}{r_1^3} = 0 \text{ and } n^2\mu - \frac{\mu}{r_2^3} - \frac{9I}{2r_2^5} = 0. \tag{9}$$

As $0 < p, I << 1$, hence for the first approximation $p = 0 = I$ and the solutions of Equation (9) are given by

$$-n^2 + \frac{1}{r_1^3} = 0 \text{ and } n^2 - \frac{1}{r_2^3} = 0$$

i.e.,

$$r_1 = r_2 = n = 1.$$

This is possible only when both the primaries are of equal masses. But the masses of the Sun and Jupiter are not equal so $r_1 \neq r_2$. For better approximation we assume $p \neq 0$ and $I \neq 0$, hence the solution of Equation (9) may be supposed to be

$$r_1 = 1+\alpha \text{ and } r_2 = 1+\beta, \tag{10}$$

where α, β are distinct but very small quantities, i.e., $0 < \alpha, \beta << 1$.

Neglecting higher order terms of α, β and coupling terms $\alpha \times \beta$, one can find the values of x and y; by using the Equation (10) as

$$\left.\begin{aligned} x &= \mu - \frac{1}{2} - \alpha + \beta, \\ y &= \pm \frac{\sqrt{3}}{2}\left\{1 + \frac{2(\alpha+\beta)}{3}\right\}, \end{aligned}\right\} \tag{11}$$

i.e.,

$$L_{4,5} = \left[\mu - \frac{1}{2} - \alpha + \beta,\ \pm \frac{\sqrt{3}}{2}\left\{1 + \frac{2(\alpha+\beta)}{3}\right\}\right].$$

Putting the values of n and r_1 in the first equation of System (9) and neglecting the higher order and coupling terms, we get $\alpha = -\frac{I}{2}$.
Similarly, from the second equation of System (9), we get

$$\beta = -\frac{I}{2} + \frac{p}{3} + \frac{3I}{2\mu}.$$

Hence, the co-ordinates of triangular libration points $L_{4,5}$ are given by

$$L_{4,5} = \left[\mu - \frac{1}{2} + \frac{p}{3} + \frac{3I}{2\mu},\ \pm \frac{\sqrt{3}}{2}\left\{1 + \frac{2p}{3} + \frac{(3-2\mu)I}{3\mu}\right\}\right].$$

4. Critical Mass

The characteristic equation for equilateral triangular libration points can be written as

$$\lambda^4 + \left(4n^2 - \Omega^0_{xx} - \Omega^0_{yy}\right)\lambda^2 + \left(\Omega^0_{xx}\Omega^0_{yy} - \Omega^{0\ 2}_{xy}\right) = 0, \tag{12}$$

where

$$\Omega^0_{xx} = \frac{3}{4} - \frac{(7-6\mu)}{4}p + \frac{3(29\mu-12)}{8\mu}I, \tag{13}$$

$$\Omega_{yy}^{0} = \frac{9}{4} - \frac{(5-6\mu)}{4} p + \frac{3(12+7\mu)}{8\mu} I, \tag{14}$$

and

$$\Omega_{xy}^{0} = \frac{\sqrt{3}}{8}\left[-6 + 12\mu + \frac{1}{3}\left(\frac{26}{8} - 40\mu \right) p + \left(\frac{12 + \mu + 22\mu^2}{\mu} \right) I \right]. \tag{15}$$

Here $\Omega_{xx}^{0}, \Omega_{yy}^{0}, \Omega_{xy}^{0}$ are the values of $\Omega_{xx}, \Omega_{yy}, \Omega_{xy}$ respectively at the libration points.

If $\lambda^2 = \Lambda$, then the reduced characteristic Equation (12) can be written as

$$\Lambda^2 + P\Lambda + Q = 0, \tag{16}$$

where

$$P = 4n^2 - \Omega_{xx}^{0} - \Omega_{yy}^{0} = 1 - p - \frac{15I}{2}, \tag{17}$$

$$Q = \Omega_{xx}^{0}\Omega_{yy}^{0} - \Omega_{xy}^{0\,2} = \frac{27\mu(1-\mu)}{4} - 15\mu(1-\mu)p + \frac{9}{4}\left(6 + 5\mu - 11\mu^2\right) I. \tag{18}$$

For commensurability, let k^2 be the ratio of the roots of the reduced characteristic Equation (16). Then

$\frac{\Lambda_1}{\Lambda_2} = \frac{P - \sqrt{P^2 - 4Q}}{P + \sqrt{P^2 - 4Q}} = \frac{1}{k^2}$, where k is a positive integer.

That is,

$$P^2 k^2 - \left(k^2 + 1\right)^2 Q = 0. \tag{19}$$

The combination of the Equations (17), (18) and (19) yields

$$3\left(k^2+1\right)^2 \left(9 - 20p + 33I\right)\mu^2 - 3\left(k^2+1\right)^2 \left(9 - 20p + 15I\right)\mu + 4k^2\left(1 - 2p - 15I\right) = 0. \tag{20}$$

The roots of Equation (20) are called critical mass denoted by μ_c and given by

$$\mu_c = \frac{3\left(k^2+1\right)\left(9 - 20p + 15I\right) \pm \sqrt{81\left(k^2+1\right)^2\left(9 - 40p + 30I\right) - 48}}{6\left(k^2+1\right)\left(9 - 20p + 33I\right)}. \tag{21}$$

Putting $p = 0$, we get

$$\mu_c = \frac{3\left(k^2+1\right)\left(9+15I\right) \pm \sqrt{81\left(k^2+1\right)^2\left(9+30I\right)-48}}{6\left(k^2+1\right)\left(9+33I\right)}$$ [Same as Hassan et al. (2013)]

and by putting $p = I = 0$, we get

$$\mu_c = \frac{1}{2}\left[1-\sqrt{\left(1-\frac{16k^2}{27\left(k^2+1\right)^2}\right)}\right].$$ [Same as Szebehely (1981) and Tuckness (1995)]

5. Numerical Integration

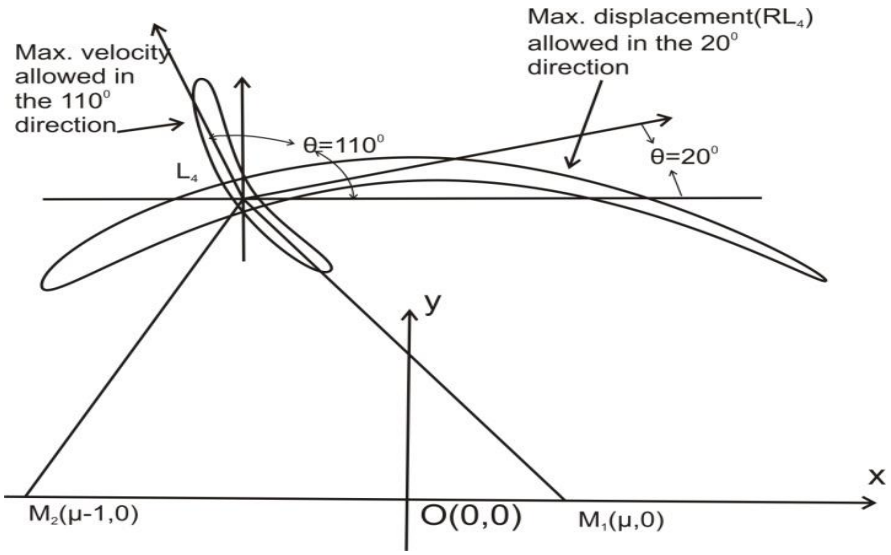

Figure 1. Maximum velocity and Maximum displacement Envelopes

For numerical integration, let us introduce $x-\mu = x_1, y = x_2, \dot{x} = x_3, \dot{y} = x_4$ and reducing two second order differential equation of motion given in Equation (1) to the four first order differential equations as

$$\left.\begin{aligned} \frac{dx_1}{dt} &= x_3, & \frac{dx_2}{dt} &= x_4, \\ \frac{dx_3}{dt} &= 2nx_4 + \frac{\partial\Omega}{\partial x_1}, & \frac{dx_4}{dt} &= -2nx_3 + \frac{\partial\Omega}{\partial x_2}, \end{aligned}\right\} \tag{22}$$

where

$$\Omega = \frac{n^2}{2}\left[\left(1-\mu\right)r_1^2 + \mu r_2^2\right] + \frac{\left(1-p\right)\left(1-\mu\right)}{r_1} + \frac{\mu}{r_2} + \frac{3I}{2r_2^3}, \tag{23}$$

with

$$r_1^2 = x_1^2 + x_2^2 \text{ and } r_2^2 = (x_1 + 1)^2 + x_2^2.$$

If p_1 and p_2 are the momenta corresponding to the co-ordinates (x_1, x_2) of the infinitesimal mass, then $p_1 = \dot{x}_1 - nx_2$ and $p_2 = \dot{x}_2 + nx_1$.

The Hamilton-Jacobi equations of motion in canonical form, are

$$\left.\begin{aligned} \dot{x}_1 &= \frac{\partial H}{\partial p_1}, \quad \dot{x}_2 = \frac{\partial H}{\partial p_2}, \\ \dot{p}_1 &= -\frac{\partial H}{\partial x_1}, \quad \dot{p}_2 = \frac{\partial H}{\partial x_2}, \end{aligned}\right\} \tag{24}$$

with the corresponding Hamiltonian

$$H = \frac{n^2}{2}\left(p_1^2 + p_2^2\right) + \left(p_1 x_2 - p_2 x_1\right) - \frac{(1-p)(1-\mu)}{r_1} - \frac{\mu}{r_2} - \frac{3I}{2r_2^3} = C. \tag{25}$$

To solve Equation (22) numerically, we apply Runge-Kutta method within the limits given by Tuckness (1995). On construction of maximum displacement and maximum velocity envelopes of the third body, a large initial velocity is given to the third body in the direction of 110^o and integrating the trajectory for a spacecraft and amount of time and checking to show if the third body crosses the $x-$axis.

If the third body crosses the $x-$axis before the time limit, the initial velocity was decreased by 0.00001 dimensionless time units and the whole procedure was again started and continued this process until a maximum velocity was found that allowed the third body to librate around L_4 for the full length of time limit without crossing the $x-$axis. This procedure will continue for full 360^o surrounding L_4. Specifying the maximum initial velocity allowed in a certain direction constitutes a velocity vector with magnitude and direction. By connecting the end points of all such velocity vectors, we will get maximum velocity envelope.

In a similar way if the third body starts with zero initial velocity from L_4 and within specified amount of time, the third body will be at a displacement from L_4 along a certain direction without crossing the $x-$axis and then the end point of this displacement constitutes a displacement vector. This procedure will continue for all 360^o surrounding L_4. By connecting the end points, all such displacement vectors will constitute a maximum displacement envelope. The maximum velocity envelope and maximum displacement envelope are defined in the hope of showing that the third body will remain within a specified area around L_4 for an infinitely long period of time with given specific initial conditions.

6. Comparison by Poincare Surface of section

In this section, the maximum velocity and maximum displacement envelopes boundary values are investigated using time limits of Tuckness (1995) for numerical integration and Poincare surface of section. The solution of the Hamiltonian equation of motion in Equation (24) can be represented as a trajectory in a four dimensional phase space. Because of the existence of the integral of motion in Equation (25), the trajectory lays a three-dimensional subspace (H) which is equal to a constant of the phase space. The successive intersection of this three-dimensional trajectory with a two dimensional surface is called Poincare surface of section. The intersection of 3D trajectory with the surface

$$y=\frac{\sqrt{3}}{2}\left\{1+\frac{2p}{3}+\frac{(3-2\mu)}{3\mu}I\right\}$$

in the positive direction is the Poincare surface of section in our case.

In Figure 2, the Poincare surface of section has no clear visibility, so in Figure 3 (Enlarged view of Figure 2), the phase space can be divided into two regions. One region contains disconnected islands and the second region consists of primarily regular trajectories which are isolated from the islands. It means the chaotic belt of the Poincare section has been reduced due to the introduction of photogravitation and oblateness. The maximum velocity and maximum displacements were investigated using the Poincare surface of sections for various values of μ. Initial velocities and positions from the maximum velocity and maximum displacement envelopes were numerically integrated using the Hamiltonian equations of motion and the intersection with the surface

$$y=\frac{\sqrt{3}}{2}\left\{1+\frac{2p}{3}+\frac{(3-2\mu)}{3\mu}I\right\}$$

were plotted for 500 to 2000 orbits for $y>0$ only using Runge-Kutta 7/8 integrator.

Figure 3 shows the Poincare surface of section for $\mu=0.001$, $\theta=108^{o}$ and values of initial dimensionless velocities 0.420, 0.425, 0.430, 0.435, 0.440, 0.444 for the third body orbiting at L_4, which are the same as Hassan et al. (2013). Therefore, photo-gravitation has no effect on the Poincare surface of section corresponding to maximum velocity and maximum displacement envelopes. Using stability criteria established in this study, 0.444 is the value of the maximum velocity in the direction of 108^{o}. The velocity greater than 0.444 represents unstable motion and velocity less than 0.444 represents quasi-periodic motion.

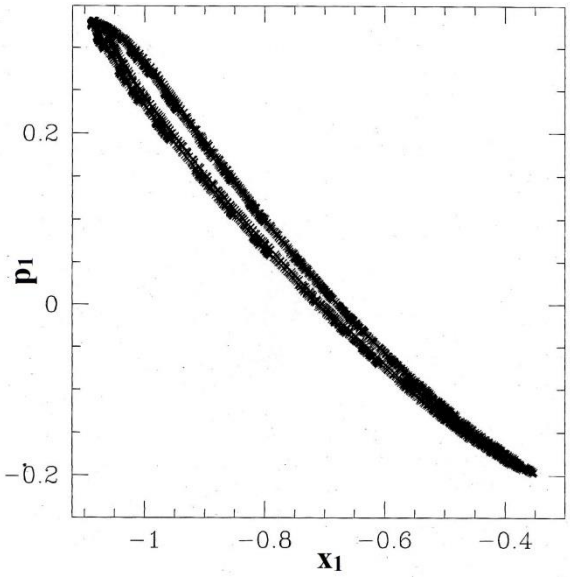

Figure 2. Surface of Poincare Section for $\mu = 0.001, \theta = 108^{o}$

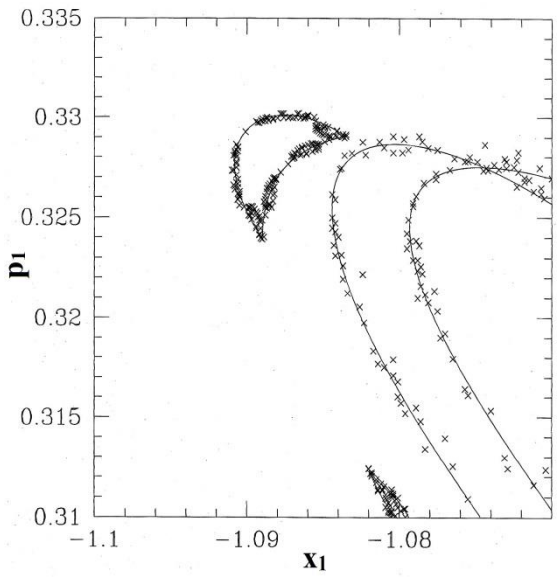

Figure 3. Enlarged view of Figure 2

Figure 4 depicts the Poincare surface of section for $\mu = 0.001, \theta = 0^{o}$ and the maximum initial displacement allowed, which can also be explored in enlarged view of Figure 4. Following Tuckness (1995), the maximum velocity and maximum displacement envelopes can be used to detect when chaotic motion of the third body is about to take place.

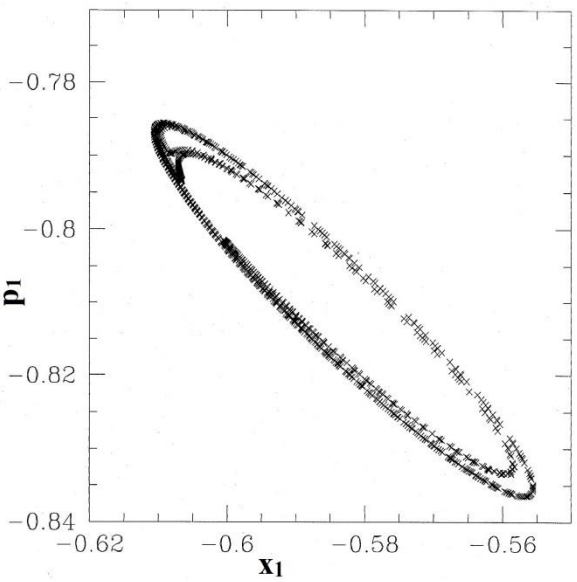

Figure 4. Surface of Poincare Section for $\mu = 0.001, \theta = 0^{o}$

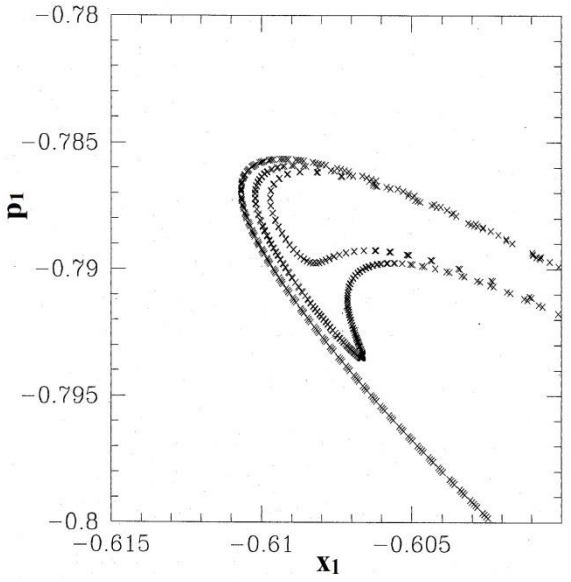

Figure 5. Enlarged view of Figure 4

7. Stability of the Infinitesimal Mass in the neighbourhood of L_4

As in Tuckness (1995), we have chosen final time $t_f = 1000$ and boundary $x-$axis, so size of the maximum velocity and maximum displacement envelopes vary according to the values

of μ, I, p and t_f under the defined boundary. Since the final time $t_f = 1000$ and boundary is the $x-$axis, hence they are assumed to be fixed and thus different envelopes vary according to μ, I and p. For the Sun-Jupiter system, we take $\mu = 0.001$ as a fixed value because we have taken Poincare sections only for two different values of θ i.e., for $\theta = 0^o$ and $\theta = 108^o$ as in Tuckness (1995) and Hassan et al. (2013).

Following Hassan et al. (2013), we have calculated the areas of displacement envelopes and velocity envelopes by considering the formula $\frac{1}{2}\int r^2 d\theta$ with the proper limits of θ for different envelopes. Because of the estimated area of the envelopes is a measure of stability, a comparison can be made on how stability varies according to the value of μ, I and p. In Figure 6, it is visible that the area of velocity envelopes became narrower in comparison to the classical case (for $I = 0$) with the increase of oblateness parameter I. Thus, the stability percentage decreases with the increase of I as in the Figure 6, the velocity envelope for $I = 0.01$ becomes the interior part of that for $I = 0.1$. In Figure 7, the displacement envelopes became narrower with very little effect of oblateness $I = 0.1$ and 0.01. We have not confirmed that, whether $I = 0.001$ have some significant effect or not on the displacement envelopes.

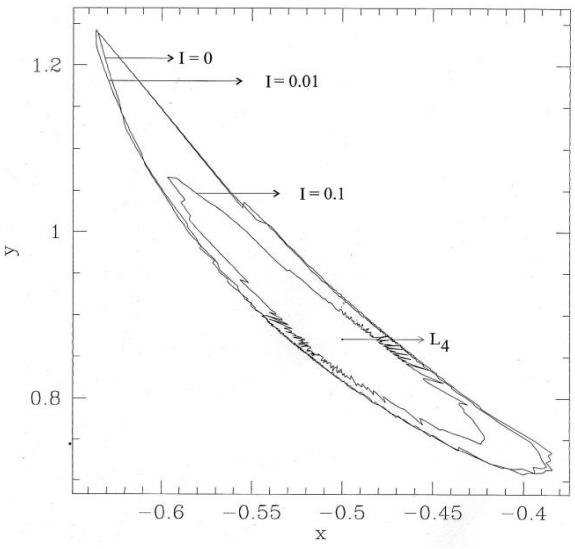

Figure 6. Maximum velocity envelopes for μ = 0.001 and I = 0, 0.01, 0.1

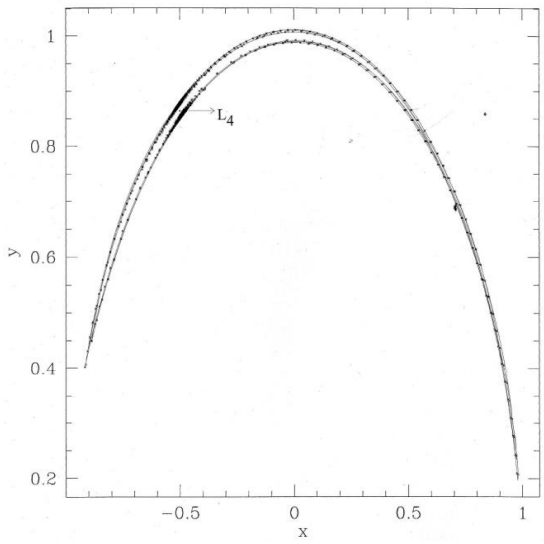

Figure 7. Maximum displacement envelopes for μ = 0.001 and I = 0, 0.01, 0.1

Figure 8 shows the position of L_4 in the common area of the velocity envelope and displacement envelope in unperturbed motion in the Sun-Jupiter system. Figure 9 depicts that the area of velocity envelopes and displacement envelopes become maximum corresponding to the same value of $\mu = 0.0009$ i.e., corresponding to this value of μ motion of the third body is most stable which means for this value of μ, the third body will librate in the neighbourhood of L_4 for maximum $t_f = 1000$ (non-dimensional time) without crossing the $x-$axis. Also, from this graph, we can conclude that for $\mu = 0.027$, both the area of velocity envelope and displacement envelopes become zero, so we can say that this value of μ is for

the most unstable motion i.e., the third body will escape from the neighbourhood of L_4 for $\mu = 0.027$.

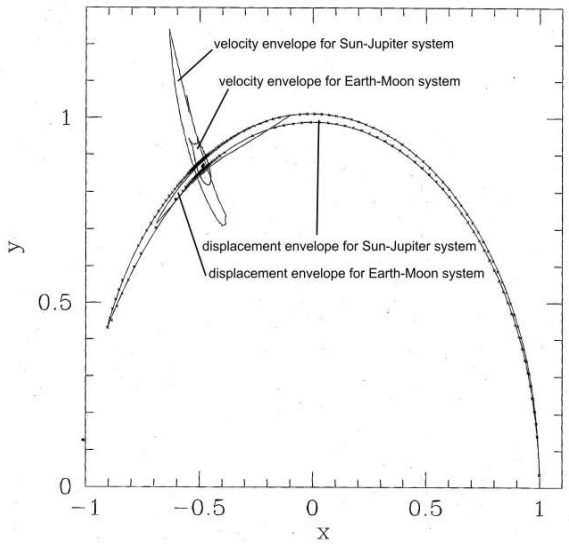

Figure 8. Maximum displacement and velocity envelopes for $\mu = 0.001 \& 0.01214$ in unperturbed motion

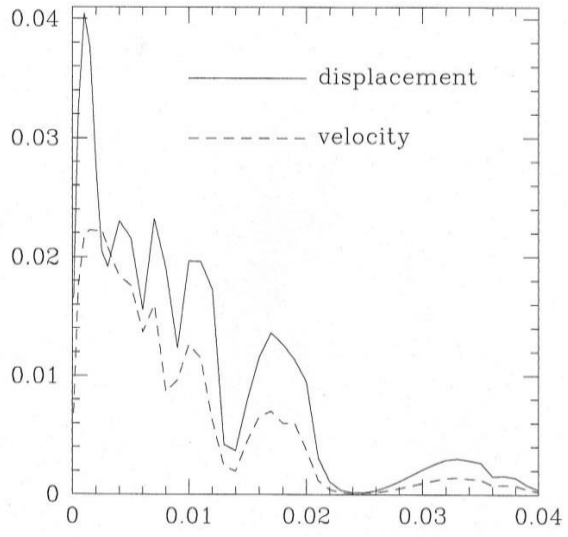

Figure 9. Area of maximum velocity and displacement in Sun-Jupiter system

8. Order of Commensurability k

Table 1. Order of Commensurability (For $I = 0$)

k	$\leftarrow \mu_c \rightarrow$						
$\downarrow$	$p = 0$	$p = 10^{-5}$	$p = 10^{-4}$	$p = 10^{-3.5}$	$p = 10^{-3}$	$p = 10^{-2.5}$	$p = 10^{-2}$
1	0.995868	0.995868	0.995866	0.995562	0.995848	0.995796	0.995547
2	0.999341	0.999341	0.999341	0.999340	0.999337	0.999319	0.999181
3	0.999835	0.999835	0.999835	0.999835	0.999833	0.999820	0.999699
4	0.999943	0.999943	0.999943	0.999943	0.999942	0.999930	0.999811
5	0.999976	0.999976	0.999976	0.999975	0.999974	0.999963	0.999845
6	0.999988	0.999988	0.999988	0.999988	0.999987	0.999975	0.999858
7	0.999993	0.999993	0.999993	0.999993	0.999992	0.999981	0.999864
8	0.999996	0.999996	0.999996	0.999996	0.999995	0.999984	0.999867
9	0.999998	0.999998	0.999998	0.999997	0.999996	0.999985	0.999868
10	0.999998	0.999998	0.999998	0.999998	0.999997	0.999986	0.999869

Table 2. Order of Commensurability (For $I = 10^{-2}$)

k	$\leftarrow \mu_c \rightarrow$						
$\downarrow$	$p = 0$	$p = 10^{-5}$	$p = 10^{-4}$	$p = 10^{-3.5}$	$p = 10^{-3}$	$p = 10^{-2.5}$	$p = 10^{-2}$
1	0.976721	0.976720	0.976717	0.976708	0.976678	0.976578	0.976181
2	0.980016	0.980016	0.980014	0.980008	0.979988	0.979920	0.979624
3	0.980485	0.980485	0.980483	0.980477	0.980459	0.980395	0.980114
4	0.980587	0.980587	0.980585	0.980580	0.980562	0.980499	0.980221
5	0.980618	0.980618	0.980616	0.980611	0.980593	0.980530	0.980253
6	0.980630	0.980630	0.980628	0.980622	0.980605	0.980542	0.980265
7	0.980635	0.980635	0.980633	0.980628	0.980610	0.980547	0.980271
8	0.980638	0.980638	0.980635	0.980630	0.980613	0.980550	0.980273
9	0.980639	0.980639	0.980637	0.980631	0.980614	0.980551	0.980275
10	0.980640	0.980640	0.980638	0.980632	0.980615	0.980552	0.980276

In the Table 1, critical mass μ_c has been calculated for $p = 0, 10^{-5}, 10^{-4.5}, 10^{-4} .....10^{-2}$ keeping $I = 0$. It is seen in the table that μ_c varies from 0.995868 to 0.995547 for $k = 1$ i.e., μ_c decreases with the increase of p. Similarly in every row of the Table 1, μ_c decreases with the increase of p for $k = 2, 3, 4.....10$ i.e., μ_c increases with the increase of commensurability k. In each column of the Table 1, μ_c increases with the increase of p from 0 to 10^{-2}.

In Figure 10, graphs show the variation of μ_c with $p = 0, 10^{-2.5}$ and 10^{-2} corresponding to each value of $k = 1, 2, 3.....10$. It is seen that μ_c increases rapidly from $k = 1, 2, 3$ whereas μ_c increases very slowly for $k = 4, 5, 6.....10$. That is, μ_c runs almost through a horizontal straight line after $k = 3$. Similar case happened in graphs of Figure 11 and Figure 12 for $I = 10^{-2}$ and $I = 10^{-1}$, respectively with a visible difference, which can be seen in Figure 11.
In Figure 13 the graphs of μ_c versus p for $I = 0, 10^{-2}$ and 10^{-1} are drawn from the first row of Tables 1, 2 and 3. It is seen that μ_c is almost constant for all values of p and $k = 1$. Similarly other graphs can be seen for $k = 2, 3, 4.....10$. All graphs almost will be horizontal lines. Therefore, photogravitation has insignificant effect on μ_c for commensurability $k = 1, 2, 3.....10$. In Figure 14, for the fixed values of $p = 10^{-5}$, the graphs of μ_c versus I for $k = 1, 2, 3.....10$ and for all values of μ_c, I, are almost same, in which μ_c decreases when I increases.

Table 3. Order of Commensurability (For $I = 10^{-1}$)

k	$\leftarrow \mu_c \rightarrow$						
$\downarrow$	$p = 0$	$p = 10^{-5}$	$p = 10^{-4}$	$p = 10^{-3.5}$	$p = 10^{-3}$	$p = 10^{-2.5}$	$p = 10^{-2}$
1	0.846665	0.846663	0.846650	0.846619	0.846519	0.846199	0.845131
2	0.848863	0.848862	0.848849	0.848820	0.848725	0.848420	0.847404
3	0.849176	0.849175	0.849163	0.849133	0.849039	0.848737	0.847728
4	0.849245	0.849243	0.849231	0.849201	0.849108	0.848806	0.847799
5	0.849265	0.849264	0.849252	0.849222	0.849128	0.848826	0.847820
6	0.849273	0.849272	0.849259	0.849230	0.849136	0.848834	0.847828
7	0.849277	0.849275	0.849263	0.849233	0.849140	0.848838	0.847832
8	0.849278	0.849277	0.849265	0.849235	0.849141	0.848839	0.847833
9	0.849279	0.849278	0.849266	0.849236	0.849142	0.848840	0.847834
10	0.849280	0.849278	0.849266	0.849237	0.849143	0.848841	0.847835

Table 4. Combined Effect of p and I on Critical Mass μ_c

k	$\leftarrow \mu_c \rightarrow$						
$\downarrow$	$p = 0,$ $I = 0$	$p = 10^{-5},$ $I = 10^{-3}$	$p = 10^{-4},$ $I = 10^{-2.5}$	$p = 10^{-3.5},$ $I = 10^{-2}$	$p = 10^{-3},$ $I = 10^{-1.5}$	$p = 10^{-2.5},$ $I = 10^{-1}$	$p = 10^{-2},$ $I = 10^{-0.5}$
1	0.995868	0.993896	0.989675	0.976708	0.939133	0.846199	0.682322
2	0.999341	0.997351	0.993092	0.980008	0.942104	0.848420	0.683466
3	0.999835	0.997843	0.993578	0.980477	0.942527	0.848737	0.683629
4	0.999943	0.997895	0.993684	0.980580	0.942619	0.848806	0.683664
5	0.999976	0.997982	0.993716	0.980611	0.942647	0.848826	0.683675
6	0.999988	0.997995	0.993728	0.980622	0.942658	0.848834	0.683679
7	0.999993	0.998000	0.993734	0.980628	0.942662	0.848838	0.683681
8	0.999996	0.998003	0.993736	0.980636	0.942665	0.848839	0.683682
9	0.999998	0.998004	0.993738	0.980631	0.942666	0.848840	0.683682
10	0.999998	0.998005	0.993739	0.980632	0.942666	0.848841	0.683683

In Table 4, critical mass has been calculated by the formulae given in Equation (21) when both of p and I are allowed to vary. For $\left(p = 10^{-5}, I = 10^{-3}\right), \left(p = 10^{-4}, I = 10^{-2.5}\right)$ $\left(p = 10^{-3.5}, I = 10^{-2}\right), \left(p = 10^{-3}, I = 10^{-1.5}\right), \left(p = 10^{-2.5}, I = 10^{-1}\right)$ and $\left(p = 10^{-3.5}, I = 10^{-2}\right)$, μ_c has been calculated for $k = 1, 2, 3.....10$ and graphs were plotted in Figure 15. In this figure, all pairs of p and I represent almost the same graph with a slight difference. With the increase of both the parameter p and I together, μ_c decreases. Thus, by the reduction of critical mass μ_c, stability range of the triangular libration points is reduced according to the criterion under consideration.

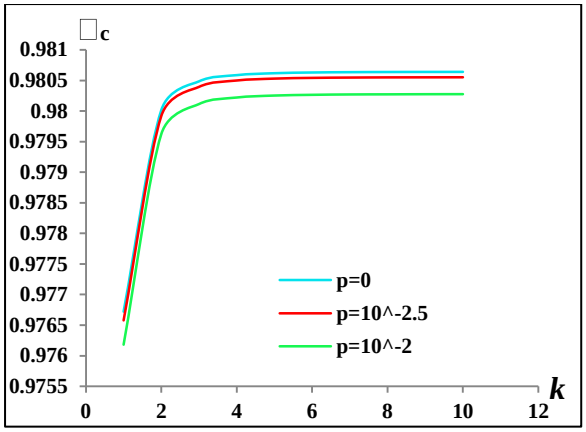

Figure 10. Plotting of μ_c vs. k for $I=0$

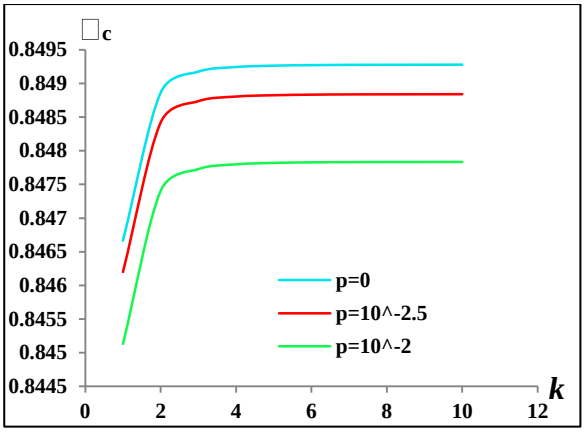

Figure 11. Plotting of μ_c vs. k for $I=10^{-2}$

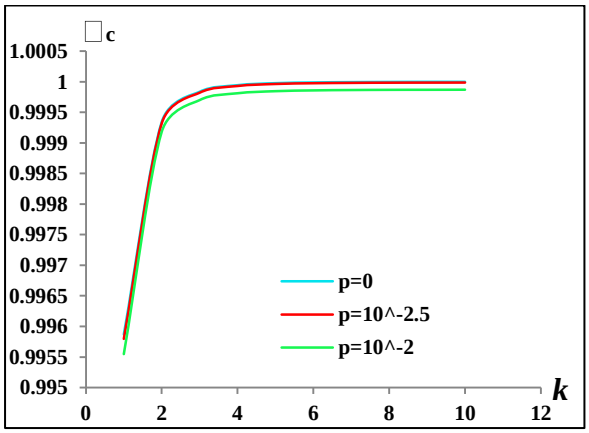

Figure 12. Plotting μ_c vs. k for $I=10^{-1}$

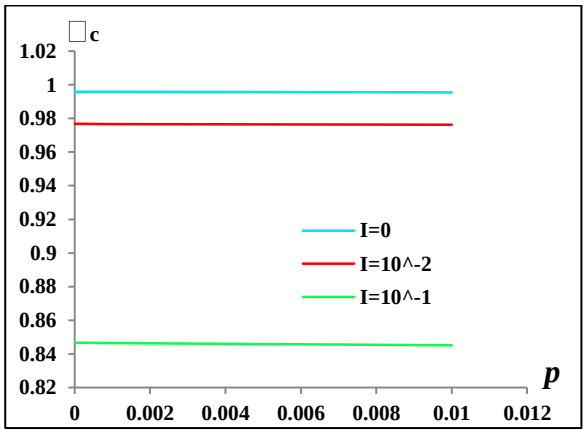

Figure 13. Plotting μ_c vs. p for $k=1$

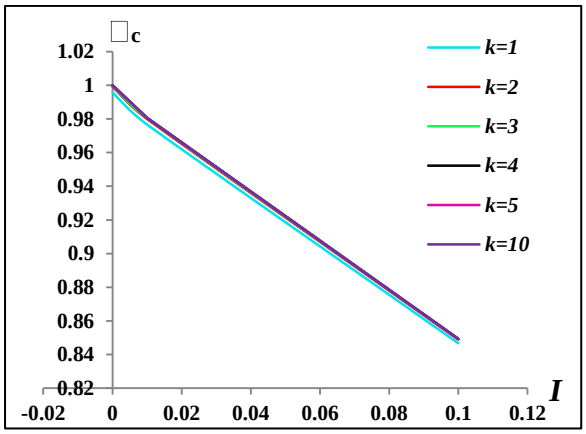

Figure 14. Plotting μ_c vs. I for $p=10^{-5}$

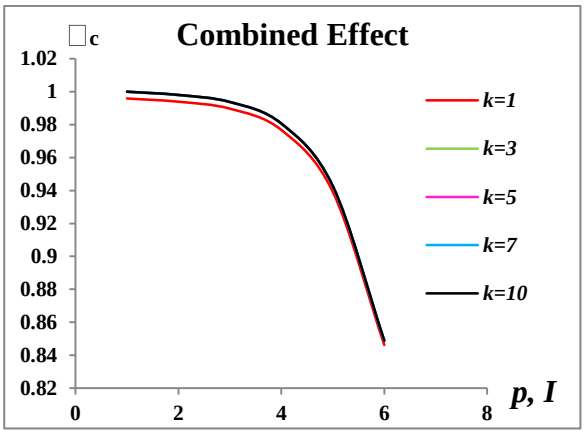

Figure 15. Combined Effect of p and I on μ_c

9. Conclusion

The present study aims to check the joint effect of solar radiation of the Sun and oblateness of the Jupiter on the stability of the triangular libration points $L_{4,5}$ in the Sun-Jupiter system. In sections 2, 3 and 4 of the present work, all mathematical derivations are given, which are required to discuss the stability of the triangular libration points. In section 5, for numerical integration we have applied fourth-order Runge-Kutta method with a seventh-order automatic step-size control in the FORTRAN programming for solving the four first-order differential equations of the system (22).

In section 6, with the techniques given by Tuckness (1995), we have produced data of $x_1, x_2, \dot{x}_1, \dot{x}_2, C$, then within the time limit of Tuckness, Poincare surface of section are plotted in Figures 3, 4 and 5. In classical case of Tuckness (1995), the regions of motion in Poincare surface of section can be divided into three regions. In the first region, all trajectories are regular and periodic, in the second region trajectories are quazi-periodic and in the third region chaotic belt is seen in which islands are scattered throughout the region of motions but in our case, there is a significant change in the chaotic region for both the case of $\theta = 0,\ \theta = 108^{o}$. In the chaotic region of our Poincare surface of section, the scattered islands have been significantly reduced. Thus, the chaotic belt has been reduced due to the introduction of the photogravitation of the Sun and oblateness of Jupiter.

In section 7, we have compared the stability criterion of the third body in the vicinity of the triangular libration points with that of the classical case given by Tuckness (1995). In Figure 6, the area of velocity envelopes is maximum for $I = 0$ but for $I = 0.01$, the area of velocity envelopes has been reduced and for $I = 0.1$, the area of velocity envelopes is further reduced; i.e., by increasing the oblateness parameter I, the area of velocity envelopes decreases. In other words, we can say that due to oblateness of Jupiter, the percentage of stability of triangular libration points reduced; i.e., oblateness of the Jupiter has a significant effect on the stability of triangular libration points of the Sun-Jupiter system but no significant effect of photogravitation is seen in the area of velocity envelopes. As far as the area of displacement envelopes is concerned, no effect of photogravitation and oblateness is found, which is visible in Figure 7 and 8; i.e., due to photogravitation of the Sun and oblateness of the Jupiter, the area of the displacement envelopes is not reduced.

From all the sections discussed above and the graphs drawn in Figures 10, 11, 12, 13, 14 and 15, we conclude that a great effect of oblateness and a very little effect of photogravitation have reduced the range of stability of the triangular libration points in comparison of the classical case.

Acknowledgement

We are very thankful to the UGC (University Grants Commission), ERO, Kolkata and New Delhi, India *for sanctioning the Minor Research Project and supporting the execution of such important research.*

REFERENCES

Alfriend, K.T. (1970). The Stability of the Triangular Lagrangian Point's Commensurability of Order Two, Celestial Mechanics and Dynamical Astronomy, 1(3), 351-359 https://dx.doi.org/10.1007/BF01231140

Bhatnagar, K.B. and Chawla, J.M. (1977). The Effect of Oblateness of the bigger Primary on Collinear Libration Points in the restricted problem of three bodies, Celestial Mechanics and Dynamical Astronomy, 16(2), 129-136 https://dx.doi.org/10.1007/BF01228595

Breakwell, J. and Pringle, R. (1965). Resonances affecting Motion near the Earth-Moon Equilateral Libration Points. Progress in Astronautics and Aeronautics, Academic Press, New York, 17, 55-73

Deprit, A. and Deprit-Bartholome, A. (1967). Stability of the Triangular Lagrangian Points, The Astronomical Journal, 72(2), 173-179 http://articles.adsabs.harvard.edu//full/1967AJ.....72..173D/0000173.000.html

Deprit, A. and Palmore, J. (1966). Analytical continuation and first-order Stability of the short-period Orbits at L_4 in the Sun-Jupiter system, The Astronomical Journal, 71(2), 94-98 http://adsabs.harvard.edu/full/1966AJ.....71...94D

Deprit, A., Henrard, J., Palmore, J. and Price, J.R. (1967). The Trojan manifold in the system Earth-Moon, Monthly Notices of the Royal Astronomical Society, vol. 137, pp. 311-335.

Henrard, J. (1970). Concerning the genealogy of long period families at L_4, Astronomy and Astrophysics, 5, 45-52 http://adsabs.harvard.edu/abs/1970A%26A.....5...45H

Hassan, M.R., Antia, H.M. and Bhatnagar, K.B. (2013). Position and velocity sensitiveness at the Triangular Libration Points in the Restricted Problem of three bodies when the bigger Primary is an Oblate body, Astrophysics and Space Science, 346(1), 71-78 https://dx.doi.org/10.1007/s10509-013-1448-8

Leontovich, A.M. (1962). On the Stability of the Lagrange Periodic Solutions for the Restricted Problem of three bodies, Soviet Mathematics Doklady, 3, 425-428

Markeev, A.P. (1969). On the Stability of the Triangular Libration Points in the Circular bounded three-body Problem, Journal of Applied Mathematics and Mechanics, 33(1), 112-116 https://dx.doi.org/10.1016/0021-8928(69)90117-8

Markeev, A. (1973). On the Stability problem for the Lagrange solutions of the restricted three-body problem, Journal of Applied Mathematics and Mechanics, 37(4), 753-757 https://dx.doi.org/10.1016/0021-8928(73)90122-6

Markellos, V.V., Papadakis, K.E. and Perdios, E.A. (1996). Non-linear Stability zones around Triangular Equilibria in the Plane Circular Restricted three-body Problem with Oblateness, Astrophysics and Space Science, 245(1), 157-164 https://dx.doi.org/10.1007/BF00637811

McKenzie, R. and Szebehely, V. (1981). Non-linear Stability around the Triangular Libration Points, Celestial Mechanics and Dynamical Astronomy, 23(3), 223-229 https://dx.doi.org/10.1007/BF01230727

Nayfeh, A.H. (1971). Two-to-one Resonances near the Equilateral Libration Points, American Institute of Aeronautics and Astronautics Journal, 9(1), 23-27 https://dx.doi.org/10.2514/3.6119

Papadakis, K.E. (1998). Effect of Radiation on the Non-linear Stability zones of the Lagrangian Equilibrium Points, Celestial Mechanics and Dynamical Astronomy, 72(4), 235-244 https://dx.doi.org/10.1023/A:1008385311483

Pedersen, P. (1933). On the Periodic Orbits in the neighbourhood of the Triangular Equilibrium Points in the Restricted problem of three bodies, Monthly Notices of the Royal Astronomical Society, 94, 167-185

Sokolski, A.G. (1975). Stability of the Lagrange solutions of the restricted three-body Problem for the Critical ratio of the Masses, Journal of Applied Mathematics and Mechanics, 39(2), 366-369 https://dx.doi.org/10.1016/0021-8928(75)90158-6

Szebehely, V. (1967). Theory of Orbits, Academic Press, New York

Tuckness, D.G. (1995). Position and velocity sensitiveness at the Triangular Libration Points, Celestial Mechanics and Dynamical Astronomy, 61(1), 1-19 https://dx.doi.org/10.1007/BF00051686

Zsolt, S., Baliant, E. and Christo, E. (2000). The Phase Space Structure around L_4 in the Restricted three-body Problem, Celestial Mechanics and Dynamical Astronomy, 78(1), 113-123 https://dx.doi.org/10.1023/A:1011112228708